Catalysis Letters Vol. 112, Nos. 3–4, December 2006 (© 2006)
DOI: 10.1007/s10562-006-0196-6

An easy way to Pd–Zn nanoalloy with defined composition from a heterobimetallic Pd(μ–OOCMe)$_4$Zn(OH$_2$) complex as evidenced by XAFS and XRD

Olga P. Tkachenko,[a] Alexander Yu. Stakheev,[a] Leonid M. Kustov,[a] Igor V. Mashkovsky,[a] Maurits van den Berg,[c] Wolfgang Grünert,[c,*] Natalya Yu. Kozitsyna,[b] Zhanna V. Dobrokhotova,[b] Valery I. Zhilov,[b] Sergei E. Nefedov,[b] Michael N. Vargaftik,[b] and Ilya I. Moiseev[b]

[a]*N.D. Zelinsky Institute of Organic Chemistry, Russian Academy of Sciences, 119991 Moscow, Russian Federation*
[b]*N.S. Kurnakov Institute of General and Inorganic Chemistry, Russian Academy of Sciences, 119991 Moscow, Russian Federation*
[c]*Laboratory of Industrial Chemistry, Ruhr University Bochum, D-44780 Bochum, Germany*

Received 10 September 2006; accepted 20 September 2006

The heterobimetallic lantern complex Pd(μ-OOCMe)$_4$Zn(OH$_2$) was found to be readily reduced with H$_2$ under fairly mild conditions (150–250 °C, 5–10% H$_2$/He) both in the carbon-supported and crystalline states to afford a Pd–Zn nanoalloy as evidenced by the ICP elemental analysis, EXAFS, XANES and XRD data.

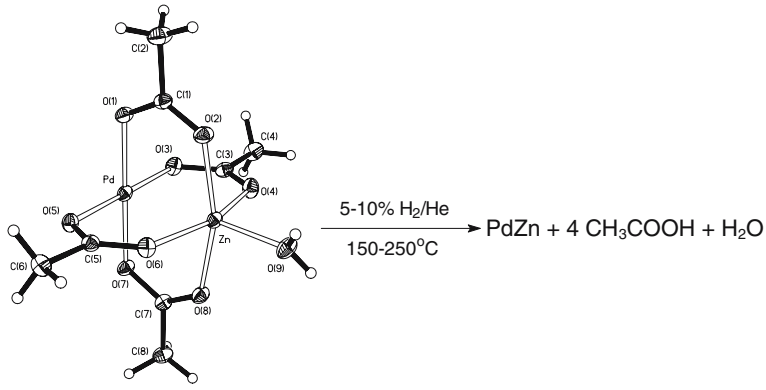

KEY WORDS: palladium; zinc; heterobimetallic complex; reduction; nanoalloy; EXAFS; XANES; XRD.

1. Introduction

Currently, much attention is paid to palladium-based heterometallic complexes due to their potential in materials science and catalysis. A traditional procedure for the preparation of supported mixed-metal catalysts comprises a separate deposition of the constituent metal precursors (normally simple metal salts) followed by redox pretreatment of the supported sample [1]. More advanced procedures make use of mixed-metal clusters (*e.g.*, heterometallic carbonyls such as $[Pd_6Ru_6(CO)_{24}]^{2-}$) as precatalysts [2]. However, synthesis and processing of such parent compounds is rather laborious. Pd-based heterobimetallic carboxylate complexes could be viable alternative precatalysts; however, until recently, there were only two well-defined examples for this type of compound – Pd_2Cd_2(μ-OOCMe)$_8$·(HOOCMe)$_2$ [3] and PdTl(μ-OOCMe)$_4$(OOCMe) [4].

A new convenient synthetic procedure developed recently in the Kurnakov Institute permits now high-yield preparations of crystalline Pd^{II}-based heterodimetallic carboxylate-bridged complexes starting from $Pd_3(OOCMe)_6$ and the complementary metal(II,III) acetates [5–7]. The complexes contain the transition (Mn^{II}, Co^{II}, Ni^{II}), post-transition (Zn^{II}) and rare-earth (Ce^{IV}, Sm^{III}, Nd^{III}, Eu^{III}) metals together with palladium. According to the single-crystal X-ray diffraction data [5], the palladium atom in each of these lantern-type complexes is strongly linked to the complementary

*To whom correspondence should be addressed.
E-mail: wahr36@mail.ru

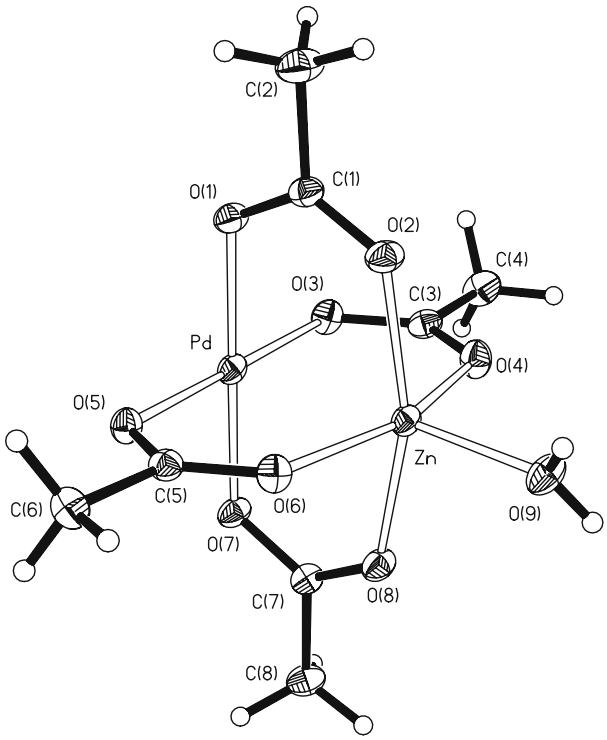

Figure 1. Molecular structure of the complex PdZn(μ-OOCMe)$_4$(OH$_2$) (**1**) by the data of single-crystal X-ray diffraction analysis [5] (Pd–Zn distance is 2.5811(6) Å, the sum of Pd and Zn covalent radii is 2.53 Å).

metal atom by four acetate bridges (see, for example, figure 1), so that the Pd – complementary metal distances (2.46–2.68 Å for 3d metals and 3.20–3.40 Å for 4f metals) are close to the sum of covalent radii, implying some metal–metal interaction. Such a structure is favorable for keeping together the constituent metal atoms during the deposition and redox treatment, giving promise for the preparation of heterometallic nanoclusters and catalysts.

Here we report on the thermal behavior and reduction with H_2 of the complex Pd(μ-OOCMe)$_4$Zn(OH$_2$) (**1**) (figure 1) in the crystalline and carbon-supported states. The Pd–Zn catalytic system deserves a special interest because it is highly active and selective in methanol synthesis, acetylene hydrogenation, steam reforming and dehydrogenation of methanol, and related industrial processes [8–12]. Pd–Zn alloys, which are thought to be crucial for the catalytic behavior, are known to form upon reduction of the Pd/ZnO catalyst at rather high temperatures ($\geq$500°C) when the catalyst was prepared according to the traditional procedure from the component salts. In this work we found that complex **1** can be readily transformed to Pd–Zn alloy nanoparticles by reduction with H_2 under much milder conditions (150–250 °C, 5–10% H_2/He), as evidenced by the data of EXAFS, XANES, XRD and ICP elemental analysis.

2. Experimental

2.1. Reagents and solvents

Solvents (glacial acetic acid and methanol, both of reagent grade) were purchased from Reakhim, Russia, and purified by standard procedures [13]. All gases (H_2, He and Ar) were of special purity grade.

The salt Zn(OOCMe)$_2\cdot$ 2H$_2$O (reagent grade) was purchased from Acros, Belgium. Palladium(II) acetate Pd$_3$(OOCMe)$_6$ was prepared by the oxidation of Pd black (prepared by reduction of $PdCl_2$ (reagent grade, purchased from Reakhim, Russia,) with $NaBH_4$) with concentrated HNO_3 in glacial acetic acid according to a known procedure [14]. The reaction product was purified from the admixture of Pd^{II} nitrate complexes by refluxing in glacial AcOH with a fresh portion of Pd black until NO_2 evolution ceased followed by recrystallization from hot AcOH.

The complex PdZn(μ-OOCMe)$_4$(OH$_2$) (**1**) was synthesized according to a procedure described in Ref [5]. The as-prepared crystals of **1** contain a THF molecule of crystallization (according to the CHN, ICP and X-ray diffraction analyses the exact formula is PdZn(μ-OOCMe)$_4$(OH$_2$)$\times$ THF), which is almost completely removed upon heating at 50–60°C for 1 h or 1 day storage in air.

The carbon mesoporous carrier "Sibunit" purchased from the TDIIC (Siberian Branch, RAS, Omsk, Russia) had the following characteristics: specific surface area (BET) is 332 m^2 g^{-1}; total pore volume is 0.45 cm^3 g^{-1}. Supported samples were prepared by the deposition of complex **1** from its methanol solution on Sibunit (1.5 wt.% based on total metals, 0.93% Pd + 0.57% Zn).

Hydrogen treatment of the unsupported PdZn acetate complex: a sample of complex **1** (98 mg, 0.230 mmol) was loaded to a quartz boat (5 $\times$ 25 mm), which was placed in a quartz tube 10 mm in diameter, connected to gas supply lines (Ar and 10% H_2/He) and put into a thermocontrolled tube oven. The tube was evacuated, filled with argon and heated to 90 °C with a rate of 5 K min^{-1} in an Ar flow (10 cm^3 min^{-1}). Then the feeding gas was changed for a 10% H_2/He gas mixture (10 cm^3 min^{-1}), the temperature was raised with a rate of 5 °C min^{-1} to 250 °C and this temperature was maintained for 2 h. Then the feeding gas was changed for Ar and the tube with the sample was slowly cooled in the oven to a room temperature in an Ar flow. According to ICP elemental analysis, the residue, an air-stable black solid powder (38.7 mg, 98% based on Pd + Zn), has the following composition: Pd, 61.12%, Zn, 36.09%. Calcd. for PdZn: Pd, 61.94%, Zn, 38.06%.

2.2. Physical measurements

The elemental C,H,N analyses were performed on an automated C,H,N-analyzer (Carlo Erba Strumentazione,

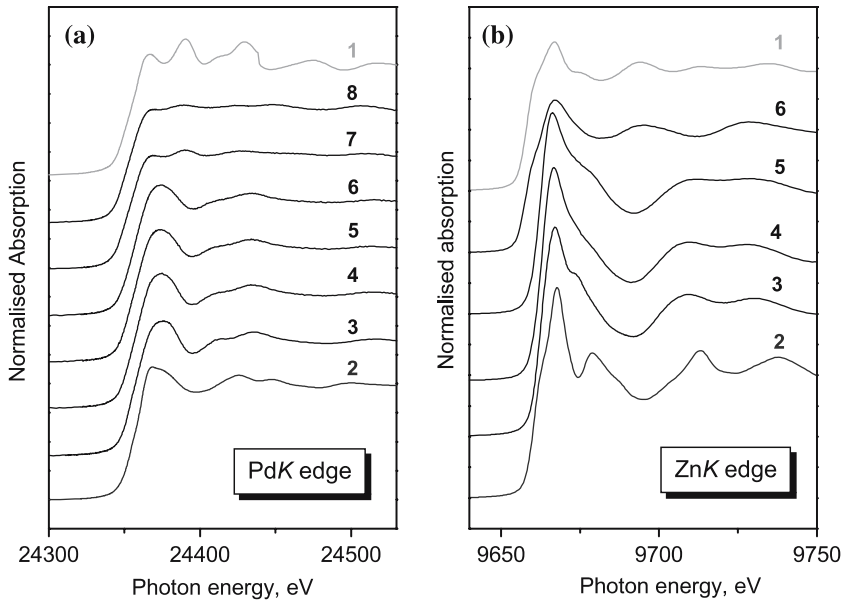

Figure 2. XANES curves of complex **1** after different treatments, (a) Pd*K* edge XANES, 1-Pd foil; 2-PdO; 3-unsupported complex **1**; 4-supported sample as prepared; 5-supported sample after treatment at 120°C under He; 6-supported sample after treatment with 5% H_2/He at 50°C; 7-supported sample after treatment with 5% H_2/He at 150°C; 8 -supported sample after treatment with 5% H_2/He at 250°C, (b) Zn*K* edge XANES, 1-Zn-foil; 2-ZnO; 3- unsupported complex **1**; 4-supported sample as prepared; 5- supported sample after treatment at 120°C under He; 6- supported sample after treatment with 5% H_2/He at 250°C.

Italy). The elemental ICP analyses were performed on an Iris Advantage instrument (Thermo Jarrell Ash, USA). Solid samples were dissolved in *aqua regia* for 3 h.

The DTA-TG analyses were performed on DSC-20 and TG-50 units of a thermoanalyzer TA-3000 (Mettler) under argon with a rate of 5 °C min^{-1}. The X-ray powder diffraction of the solid residue was measured with a Huber Imaging Plate Guinier Camera 670 (CuKα1-radiation). The X-ray patterns were indexed using the program TREOR90 [15].

XAFS measurements were carried out at HASYLAB (DESY in Hamburg, Germany) on the beamline X1 (Pd*K*-edge, 24350 eV) using a double-crystal Si(311) monochromator, which was detuned to 50% of maximum intensity to exclude higher harmonics in the X-ray beam, and on the beamline E4 (Zn*K*-edge, 9659 eV) using a double-crystal Si(111) monochromator, which was detuned to 30% of the maximum intensity to exclude higher harmonics. The spectra were recorded in the transmission mode at a low temperature (T = 80 K) in order to decrease the Debye–Waller factors. All spectra were measured simultaneously with the reference spectrum of a Pd or a Zn foil placed behind the second ionisation chamber, for calibration of the energy scale.

All experiments were performed using an *in situ* EXAFS cell described in Ref. [16], in which a fractioned sample was exposed to the flowing gas. After reduction treatment (5% H_2 in a He flow), the sample was flushed by pure helium at the same temperature to avoid the formation of palladium hydride.

To extract quantitative information from EXAFS spectra, Fourier-filtered shell contributions were fitted using the standard EXAFS formula in the harmonic approximation:

$$\chi = S_0^2 \sum_j \frac{N_j F_j(k)}{kR_j^2} \exp(-2\sigma_j^2 k^2) \sin[2kR_j + \phi_j(k)],$$

with the summation over atomic shells j. The required scattering amplitudes and phase shifts F and φ were calculated by the *ab initio* FEFF8.10 code [17]. The fitting was done in the k- and r-spaces. The shell radius R_j, coordination number N_j, Debye–Waller factor ${\sigma^2}_j$ and adjustable "muffin-tin zero" ΔE_j were determined as fitting parameters. The errors of the fitting parameters were found by decomposition of the statistical χ^2 function near its minimum, taking into account maximal pair correlations. Analysis of the EXAFS spectra was performed with the software VIPER for Windows [18].

3. Results and discussion

3.1. XANES data

Figure 2 shows the Zn*K* and Pd*K* XANES of the carbon-supported **1** after different treatments. A comparison of curves 3 and 4 in figure 2a and b suggests that that the Pd^{II}–Zn^{II} complex is not strongly perturbed in the as-prepared sample, and its heating at 120 °C under He and reduction at 50 °C in a 5% H_2/He flow produced only minor changes in the spectra.

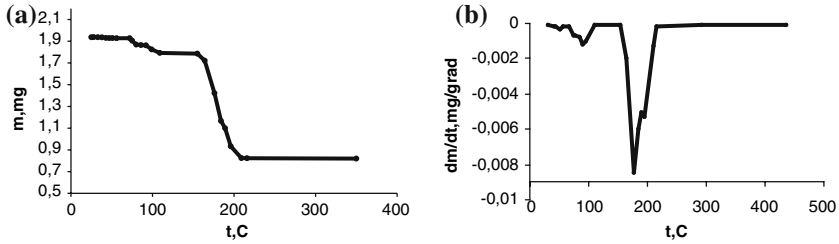

Figure 3. Thermal decomposition of unsupported complex **1** under Ar: (a) weight change; (b) differential curve.

3.2. DTA-TG data

In agreement with these results, the DTA-TG data showed only small weight changes for the unsupported complex **1** during its heating from 20 to 150 °C under Ar (figure 3). Two moderate effects were observed in this interval: (i) a weight loss of 2 ± 1.0% with a small endothermic effect ($\Delta H = 3.3 \pm 0.5$ kJ mol^{-1}) within 20–90 °C due to the removal of traces of crystallization THF molecules[†]; (ii) a weight loss of 4.3 ± 1.0% within 92–140 °C due to the removal of the coordinated H_2O molecules with an endothermic effect of 43.5 ± 5.0 kJ mol^{-1} (*cf.* $\Delta H = 40.65$ kJ mol^{-1} for water evaporation). The main structure of the tetraacetate-bridged $Pd^{II}Zn^{II}$ complex seems to maintain up to 150 °C. Essential structural changes began upon heating above this temperature: an intense weight loss with a large endothermic effect occurred in the interval 155–216 °C and terminated at 220 °C.

The total weight loss in the temperature interval 90–220 °C (56.4 ± 1.0%) corresponds, within the experimental error, to the complete removal of the acetate and water ligands to produce a mixture of Pd metal and ZnO (55.91% calculated weight loss). The ICP elemental analysis data confirmed the Pd:ZnO = 1:1 mol/mol composition of the solid residue after thermolysis (found: Pd, 56.24%, Zn 34.63%., Calcd. for PdZnO: Pd, 56.67%, Zn 34.81%).

Unlike thermolysis in inert atmosphere and low-temperature (50°C) H_2 reduction, hydrogen treatment of the supported complex **1** at 150°C produced not only Pd metal + ZnO but also another species, presumably nanoparticles of a Pd–Zn alloy. This is reflected by changes in the Pd*K*-edge XANES curves (see figure 2b, curve 7). When the supported sample was treated with 5% H_2/He at 250°C, the XANES pattern exhibited more profound changes as seen in figure 2 (a, curve 6, and b, curve 8).

[†]According to the elemental analysis and X-ray diffraction data, the as-prepared crystals of complex **1** contain one THF molecule of crystallization for the formula unit, corresponding to the exact formula $PdZn(\mu\text{-}OOCMe)_4(OH_2) \times THF$).[4] These THF molecules are easily removed upon storage of complex **1** even at room temperature for several days preceding the DTA-TG measurements. The samples under study contained 5–10% THF molecules of the original composition.

3.3. EXAFS data

The nature of these changes can be revealed by analysis of the EXAFS data (figure 4). The spectra of the unsupported and the supported complex **1** (curves 3 and 4 in figure 4a and b) show that the geometry of the complex is largely retained although the lower intensity of the scattering events at the Pd*K* edge indicates some structural distortion. The next neighbor to Pd is at ~1.6 Å (uncorrected) and weaker scattering events are at longer distances (figure 4a , curve 4). The next neighbor to Zn is at ~1.5 Å (figure 4b, curve 4). Heating the sample to 120°C in He or treatment with H_2 at 50°C does not change this structure (figure 4a, curves 5, 6, figure 4b, curve 5).

When the reduction temperature was increased to 150 and 250°C, the EXAFS pattern exhibited dramatic changes. From the Pd*K* edge EXAFS it is seen that the reduction of Palladium(II) begins at 150°C (figure 4a, curves 7 and 8), but the scattering feature of the next neighbor is different from that in the Pd foil. It has a smaller amplitude and occurs at a somewhat shorter distance ~2.3 Å (uncorrected) for reduction at 150°C, even shorter at the higher reduction temperature. No order is observed beyond the first neighbor. The Zn*K*-edge EXAFS spectrum for the sample reduced with H_2 at 250°C (figure 4b, curve 6) is different from that for Zn metal, with a pronounced peak at a distance larger than that of Zn(0)–Zn (2.45 Å compared to 2.25 Å (both uncorrected)), although the position of the edge (figure 2b, curve 6) implies that the oxidation state of the Zn atom is noticeably lower than + 2. Thus, the XAFS spectra at both the Pd and Zn*K* edges collected after H_2 reduction at 150–250°C indicate the appearance of the other element in the first shell, suggesting alloy formation. In order to check this hypothesis, model fits of the EXAFS spectra were performed, the results of which are given in figure 5 and Table 1.

The Pd*K*-edge spectra (figure 5a and b) may be readily fitted in both spaces with a single-shell model with a zinc shell around the central absorbing palladium atom. For fitting the Zn spectrum (figure 5c and d), a three-shell model was necessary: two oxygen shells and one palladium shell around the central absorbing zinc atom. It should be noted that the Pd–Zn and Zn–Pd distances practically coincide, which nicely confirms

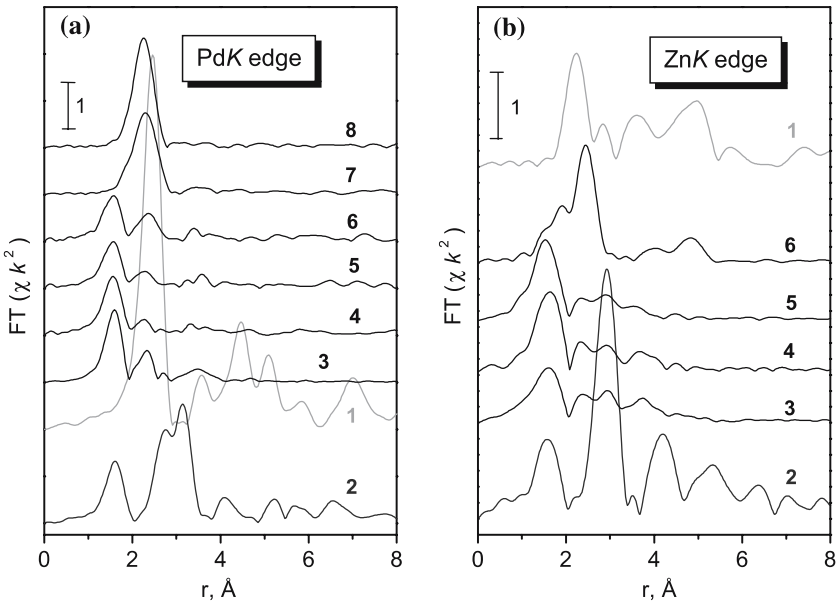

Figure 4. EXAFS spectra of carbon-supported **1** after different treatments (Fourier transform (absolute value) of k^2-weighted EXAFS function), (a) Pd*K* edge, 1-Pd foil; 2-PdO; 3- unsupported complex **1**; 4-supported sample as prepared; 5- supported sample after heating to 120°C under He; 6- supported sample after treatment with 5% H_2/He at 50°C; 7-supported sample after treatment with 5% H_2/He at 150°C; 8-supported sample after treatment with 5% H_2/He at 250°C, (b) Zn*K* edge, 1-Zn foil; 2-ZnO; 3-unsupported complex **1**; 4-supported sample as prepared; 5-supported sample after heating to 120°C under He; 6-supported sample after treatment with 5% H_2/He at 250°C.

alloy formation. As to the remaining signals in the Zn*K*-edge spectrum, the nearest O (and/or C) environment of the Zn atom in the reduced sample is similar to the first shells in the reference complex **1** and in ZnO (figure 4b, curve 4). The presence of these FT peaks implies that some Zn ions have survived after reduction in H_2 at 250°C, but those having next O neighbors have not formed an ordered oxide phase because the typical ZnO scattering pattern is absent. The fate of the Pd ions originally related to these Zn ions remains unclear, but again the formation of large (e.g. Pd metal) particles can be excluded.

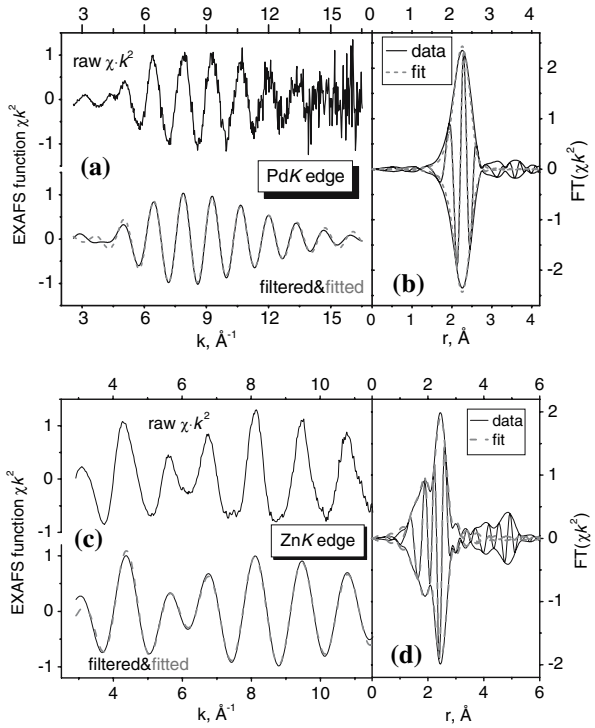

Figure 5. Model fits of Pd*K* and Zn*K* EXAFS spectra taken from carbon-supported **1** reduced with 5% H_2/He at 250°C (*cf.* figure 4a, curve 8, figure 4b, curve 6), a) and b) Pd*K* edge, *k*-space (a) and *r*-space (b), c) and d) Zn*K*edge, *k*-space (c) and *r*-space (d), for model parameters see Table 1.

The EXAFS results for the supported samples agree well with observations made upon reduction of the unsupported PdZn acetate complex **1** in hydrogen. In this experiment the crystalline complex **1** preheated under argon to 90°C was treated with a 10% H_2/He gas mixture during a temperature ramp from 90 to 250°C, kept at 250°C for 2 h and purged with Ar to destroy a Pd hydride that could also be present after the hydrogen treatment. The elemental ICP analysis showed that the solid reduction product constituted mostly of Pd and Zn in a 1:1 atomic ratio (total metal content 97.2%).

Table 1
Parameters of best model fits of spectra taken after reduction of carbon-supported **1** (5% H_2/He) at 250°C (*cf.* figure 5)

K-edge	Path	*r*(Å)	Coord. number	$10^3\ \sigma^2(Å)^{-2}$	E_0(eV)
Pd	Pd–Zn	2.588 (2)	3.7 (1)	5.8 (6)	3.9 (2)
	Zn–O	1.814 (3)	0.3 (1)	0.5 (1)	11.5 (6)
Zn	Zn–O	1.996 (1)	0.9 (1)	0.5 (1)	10.5 (2)
	Zn–Pd	2.586 (3)	3.2 (2)	4.9 (3)	3.7 (5)

The values in the parenthesis are the standard errors in the last digit.

3.4. XRD data

The XRD analysis of the solid residue revealed a single crystalline phase, a PdZn 1:1 alloy (figure 6 and Table 2). From the half-width of the diffraction lines, using the Scherrer equation $\beta\ K\lambda/L\cos\theta$, the average size of the PdZn crystallites was estimated as 25 ± 5 nm; hence, this procedure allows the preparation of metal alloy nanoparticles. The EXAFS data shown above (metal–metal coordination numbers below 4, *cf.* Table 1) show, however, that the alloy particles achieved by reduction of the carbon-supported complex are much smaller than those obtained from the unsupported complex.

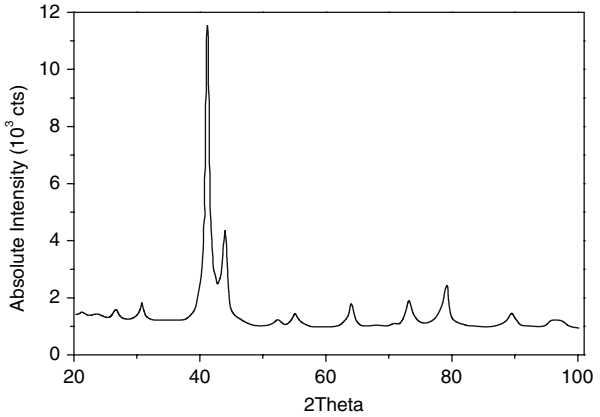

Figure 6. X-ray powder diffractogram for the solid residue after reduction of unsupported complex **1** with 10% H_2/He gas mixture at 250°C.

Table 2
XRD data for the solid residue after reduction of the unsupported complex 1 with a 10% H_2/He gas mixture at 250°C

Experiment [a]			PdZn [06–0620] [b]	
d(Å)	*I*(%)	hkl	*d*(Å)	*I*(%)
4.1674	1.61			
3.3342	3.05	001	3.32	5
2.9049	6.65	100	2.90	10
2.1891	100	101	2.19	100
2.0526	30.07	110	2.05	100
1.7481	2.50	111		
1.6643	4.78	002	1.68	30
1.4517	8.66	200	1.44	50
1.3293	0.71	201		
1.2918	9.18	112	1.30	50
1.2101	15.31	211	1.20	80
1.0932	5.34	202	1.09	50
1.0373	2.30	103	1.04	30
1.02557	2.80	220	1.02	30

[a]Symmetry: Tetragonal P; $a = 2.9004(15)$ Å; $c = 3.3292(20)$ Å; $V = 28.01(3)$ Å^3.
[b]Indexed by the program TREOR 90.[9]

4. Conclusions

This study showed that the palladium–zinc alloy nanoparticles can be formed by reduction of Pd^{II} and Zn^{II} under rather mild conditions when the Pd^{II}–Zn^{II} heterometallic carboxylate complex **1** is used as a parent compound. This result can be due to the fact that the tetrabridged structure of complex **1** is rather stable even at elevated temperatures, up to 100–150°C, keeping the Pd and Zn atoms together under conditions of hydrogen treatment (150–250°C). The reduction easily proceeds at low H_2 partial pressures (0.05–0.10 atm), under much milder conditions than have been used in traditional preparation procedures [9, 11]. These facts demonstrate the advantage of using heterometallic carboxylate complexes as parent compounds for the synthesis of nanoalloys and mixed-metal catalysts.

Acknowledgments

The authors thank the Russian Foundation for Basic Research (Projects Nos. 05-03-32683, 05-03-32794, 06-03-32578 and 06-03-08173), the Program of the President of the Russian Federation for Support of Leading Russian Scientific Schools (grant NSh-4959.2006.03), the Program of the Russian Academy of Sciences for Basic Research "Purposeful Synthesis of Inorganic Substances and Creation of Related Functional Materials", the International Science and Technology Center ISTC-1764 Grant and HASYLAB (DESY, Germany) for X-ray beamtime (project I-05-041).

References

[1] J.H. Sinfelt, *Bimetallic Catalysts. Discoveries, Concepts and Applications* (Wiley, New York, 1983).
[2] J.M. Thomas, B.F.G. Johnson, R. Raja, G. Sankar and P.A. Midgley, Acc. Chem. Res. 36 (2003) 20.
[3] S. Adam, A. Bauer, O. Timpe, U. Wild, G. Mestl, W. Bensch and R. Schlögl, Chem. Eur. J. 4 (1998) 1458.
[4] A.L. Balch, B.J. Davis, E.Y. Fung and M.M. Olmstead, Inorg. Chim. Acta 212 (1993) 149.
[5] N.Yu. Kozitsyna, S.E. Nefedov, F.M. Dolgushin, N.V. Cherkashina, M.N. Vargaftik and I.I. Moiseev, Inorg. Chim. Acta 359 (2006) 2072.
[6] N.Yu. Kozitsyna, S.E. Nefedov, N.V. Cherkashina, V.N. Ikorski, M.N. Vargaftik and I.I. Moiseev, Russ. Chem. Bull. 54 (2005) 2215.
[7] N.Yu. Kozitsyna, S.E. Nefedov, M.N. Vargaftik and I.I. Moiseev, Mendeleev Commun. 15 (2005) 223.
[8] N. Iwasa, N. Ogawa, S. Masuda and N. Takezawa, Bull. Chem. Soc. Jpn 71 (1998) 1451.
[9] N. Iwasa, T. Mayanagi, S. Masuda and N. Takezawa, React. Kinet. Catal. Lett. 69 (2000) 355.
[10] N. Iwasa, H. Suzuki, M. Terashita, M. Arai and N. Takezawa, Catal. Lett. 96 (2004) 75.
[11] S. Liu, K. Takahashi, K. Uematsu and M. Ayabe, Appl. Catal. A 227 (2004) 265–270; 2005,283, 125–135.

[12] S. Liu, K. Takahashi, K. Fuchigami and K. Uematsu, Appl. Catal. A 299 (2006) 58.
[13] D. Perrin and W.L.F. Armarego, *Purification of Laboratory Chemicals* 3 ed.(Pergamon, Oxford, 1988).
[14] T. A. Stephenson, S. M. Morehouse, A. R. Powell, J. P., Heffer and G.Wilkinson, J. Chem. Soc. (1965) 3632.
[15] P.-E. Werner, L. Eriksson and M. Westdahl, J. Appl. Crystallogr. 18 (1985) 367.
[16] F.W.H. Kampers, T.M.J. Maas, J. van Groondele, D.C. Brinkgreve and D.C. Koningsberger, Rev. Sci. Instrum. 60 (1989) 2635.
[17] A.L. Ankudinov, B. Ravel, J.J. Rehr and S.D. Conradson, Phys. Rev. B 58 (1998) 7565.
[18] K.V. Klementiev, VIPER for Windows (Visual Processing in EXAFS Researches), freeware, http://www.desy.de/~klmn/viper.html.